New semiconducting silicide Ca_3Si_4

2007 J. Phys.: Condens. Matter 19 346207

(http://iopscience.iop.org/0953-8984/19/34/346207)

IOP PUBLISHING JOURNAL OF PHYSICS: CONDENSED MATTER

J. Phys.: Condens. Matter **19** (2007) 346207 (8pp) doi:10.1088/0953-8984/19/34/346207

New semiconducting silicide Ca_3Si_4

D B Migas[1], V L Shaposhnikov[1], A B Filonov[1], N N Dorozhkin[2] and V E Borisenko[1]

[1] Belarusian State University of Informatics and Radioelectronics, P. Browka 6, 220013 Minsk, Belarus
[2] Belarusian State University, Nezavisimosti ave. 4, 220050 Minsk, Belarus

E-mail: migas@mater.unimib.it

Received 26 March 2007, in final form 4 June 2007
Published 20 July 2007
Online at stacks.iop.org/JPhysCM/19/346207

Abstract

By means of *ab initio* calculations we have revealed a newly discovered Ca_3Si_4 compound to be a semiconductor. It is characterized by an indirect transition of 0.35 eV. A peculiar dispersion of the last valence band and the first conduction band, displaying a loop of extrema, has been found. This feature leads to large anisotropy of the mobility of holes and electrons. We also present the dielectric function of this material in comparison with data for another semiconducting calcium silicide Ca_2Si.

(Some figures in this article are in colour only in the electronic version)

1. Introduction

Semiconducting silicides have been intensively investigated because of their potential use in thermoelectric and optoelectronic applications [1]. Much attention has focused on transition metal silicides like β–$FeSi_2$, while compounds of silicon with alkaline-earth metals (Mg, Ca, Ba) have been less studied. Among the latter only Mg_2Si and $BaSi_2$ have been reported to be semiconductors [1]. Recently, by means of *ab initio* calculations, we have shown that Ca_2Si also displays semiconducting properties [2]. This issue has been confirmed by calculations within the GW approximation [3], indicating that the appearance of a new semiconducting compound in the Ca–Si system is not excluded. In fact, the phase diagram of the Ca–Si system was reinvestigated by Manfrinetti *et al* [4] and a new compound—Ca_3Si_4—was found. It crystallizes in the hexagonal structure (space group $P6_3/m$) and has the following lattice constants: $a = 8.541$ Å and $c = 14.906$ Å. The unit cell consists of six formula units where Ca and Si atoms are grouped respectively into four inequivalent sites. To the best of our knowledge there is no information about electronic and optical properties of Ca_3Si_4, and this inspired us to perform a theoretical study. Thus, in this paper we will present the band structure, density of states and the real and imaginary part of the dielectric function of Ca_3Si_4 as calculated by different first principles methods in addition to our predictions on the hole mobility with temperature.

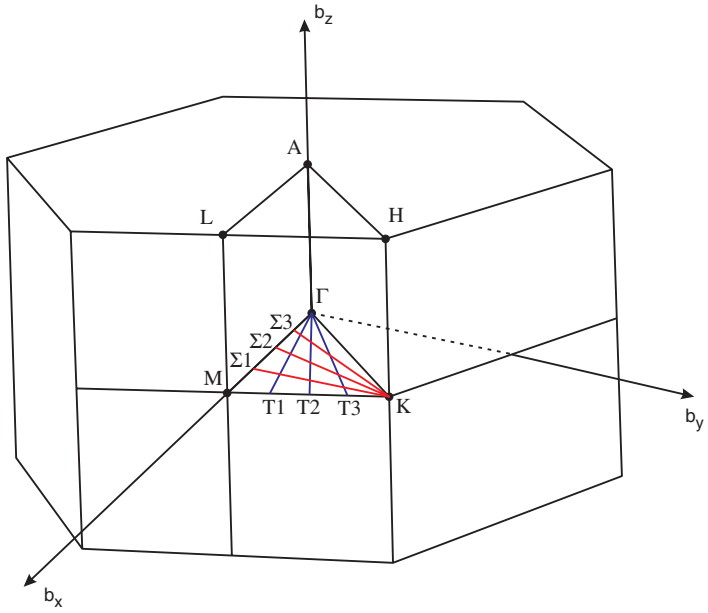

Figure 1. The hexagonal Brillouin zone.

2. Computational details

The first principles total energy code VASP with a plane-wave basis-set and ultrasoft pseudopotentials (USPP), described in detail elsewhere [5, 6], was used for full structural optimization. We applied exchange and correlation potentials using the local density approximation (LDA) of Ceperly and Alder as parameterized by Perdew and Zunger [7], and the generalized gradient approximation (GGA) of Perdew and Wang [8]. Total energy minimization, via an optimization of the lattice parameters and a relaxation of the atomic positions in a conjugate gradient routine, was obtained by calculating the Hellmann–Feynman forces and the stress tensor. The Pulay corrections have been included in order to compensate for changes of the basis set due to a variation in the shape of the unit cell. We set the energy cutoff at 330 eV and used a $7 \times 7 \times 3$ grid of Monkhorst–Pack points. The atomic relaxation was stopped when forces on atoms were less than 0.01 eV Å^{-1}. To ensure convergence the final iterations were performed on a $9 \times 9 \times 5$ grid. The calculation of band structures was carried out on the obtained self-consistent charge densities.

The electronic band structure and dielectric function have been calculated by using a full-potential linearized augmented plane wave method (FLAPW) realized in the WIEN2k package [9]. We applied the same GGA approximation [8] along with the structural parameters fully optimized by USPP. The self-consistent procedure was carried out with the energy cut-off constant $R_{MT} \cdot K_{\max} = 7$ and on the mesh of 36 **k**-points in the irreducible part of the Brillouin zone shown in figure 1. The integration on the Brillouin zone was performed by the tetrahedron method with Blöchl corrections. A dense mesh of 686 **k**-points was generated to calculate the total and projected densities of states (DOS) as well as the dipole matrix elements and the imaginary and real parts of the dielectric function. The effective mass tensors for holes and electrons were evaluated along the principal axes of the ellipsoidal energy surface in the band extrema by calculating the appropriate second derivatives within the five-point approximation.

Table 1. Optimized lattice constants (in Å) and their ratios as calculated by USPP in comparison with experimental data [4].

	a	c	a/c
Theory (LDA)	8.359	14.550	0.575
Theory (GGA)	8.534	14.881	0.573
Experiment	8.541	14.906	0.573

Table 2. Theoretical atomic coordinates (fractional positions in units of the primitive translation vectors), obtained by USPP with the GGA along with experimental data [4].

	x		y		z	
	Experiment	Theory	Experiment	Theory	Experiment	Theory
Ca(1)	0.4212	0.4215	0.3287	0.3280	0.0975	0.0976
Ca(2)	1/3	1/3	2/3	2/3	1/4	1/4
Ca(3)	0	0	0	0	0	0
Ca(4)	0	0	0	0	1/4	1/4
Si(1)	0.0898	0.0909	0.3522	0.3540	0.1102	0.1098
Si(2)	0.3831	0.3815	0.0558	0.0559	1/4	1/4
Si(3)	1/3	1/3	2/3	2/3	0.0568	0.0571
Si(4)	2/3	2/3	1/3	1/3	1/4	1/4

3. Results and discussion

3.1. Optimization of the crystal structure

The lattice parameters as optimized by USPP with LDA and GGA in comparison with experimental data are summarized in table 1. It is evident that LDA sizeably underestimates the lattice constants whereas the GGA predictions, while still underestimated, are very close to experimental values. In order to compare theoretical (zero temperature) and experimental (room temperature) results, the corresponding thermal expansion coefficients (which are unknown) should be taken into account. Thus, in the case of Ca_3Si_4 GGA is a preferable choice. In addition to that, in table 2 we also present optimized atomic coordinates calculated with the GGA; these are found to differ only in the third or forth significant digit with respect to the experimental ones. It should also be mentioned that the atomic coordinates as optimized by LDA (not shown here) are very closed to experimental results. This effect can be explained by the fact that both LDA and GGA predict the correct a/c ratio (table 1) even though LDA provides the smaller equilibrium volume.

3.2. Band structure and density of states

The band structure of Ca_3Si_4 along some high-symmetry directions in the Brillouin zone is shown in figure 2. It displays the indirect band-gap of 0.37 eV: the valence band maximum locates at $0.4 \times \Gamma$–M and the conduction band minimum stands at $0.7 \times$ M–K. It is clearly seen that the last valence band possesses two well-pronounced maxima at $0.4 \times \Gamma$–M and $0.6 \times$ K–Γ separated by a few meV. The first conduction band is also characterized by two minima at $0.7 \times$ M–K and $0.2 \times$ K–Γ, which are close in energy, in addition to a very small dispersion of the band along the M–L and H–K directions. In order to clarify the position of the valence band maximum we have calculated band structures along Γ–M, Γ–T1, Γ–T2, Γ–T3 and Γ–K (see the corresponding segments of the Brillouin zone in figure 1) which are presented in figure 3. Strictly speaking, the maximum along the Γ–T2 segment is found to be 20 meV higher in

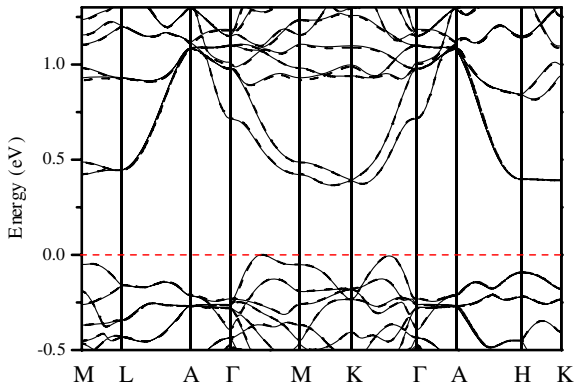

Figure 2. Band structure of Ca_3Si_4 along some symmetry directions of the Brillouin zone (see figure 1) as calculated by FLAPW (solid line) and USPP (dashed line).

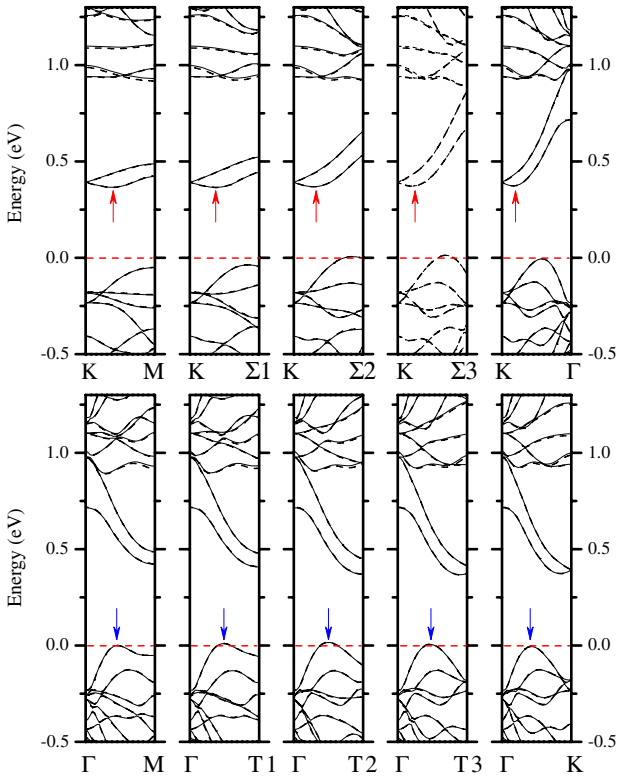

Figure 3. Band structure of Ca_3Si_4 along Γ–M, Γ–T1, Γ–T2, Γ–T3, Γ–K and K–Γ, K–Σ1, K–Σ2, K–Σ3, K–M segments (see figure 1) indicating the loop of extrema for the last valence band and the first conduction band, respectively. The solid and dashed lines correspond to the FLAPW and USPP calculations, respectively. Arrows show the position of the local maxima/minima along each segment.

energy with respect to the one along Γ–M, leading to an indirect gap of 0.35 eV. In addition, all maxima of the last valence band along each segment indicated by arrows in figure 3 are

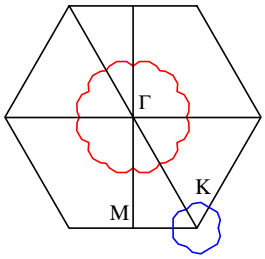

Figure 4. The map of the loops of extrema in the Brillouin zone around the Γ (valence band) and K (conduction band) points.

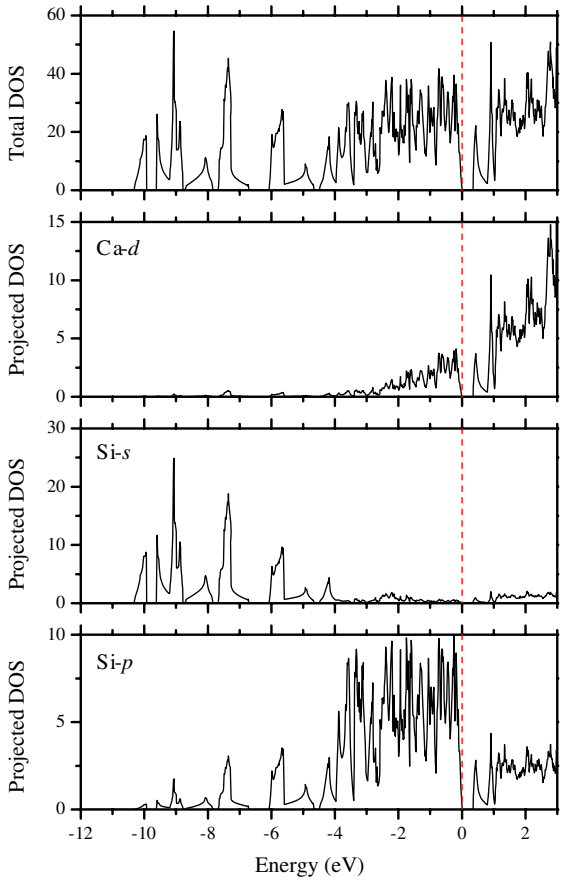

Figure 5. The total and projected DOS (states/eV/cell) of Ca_3Si_4 as calculated by FLAPW. The vertical dashed line corresponds to the Fermi level, which is set to zero energy.

very close in energy, as if the loop of extrema is formed around the Γ point (figure 4). Similar effects can be traced for the first conduction band where the loop of extrema is found around the K point (see figures 3 and 4). We do not think that the loop of extrema is an unique feature of the Ca_3Si_4 band structure because it could be present for iron monosilicide FeSi (compare the dispersion of the last valence band and the first conduction band along the M–Γ and Γ–R

Table 3. The principal axis components of the effective mass tensor for holes and electrons in units of the free-electron mass.

Holes			Electrons		
m_{xx}	m_{yy}	m_{zz}	m_{xx}	m_{yy}	m_{zz}
0.46	$\gg 1$	0.83	$\gg 1$	0.70	1.01

segments in figure 6 of [10]). It should be mentioned here that both USPP and FLAPW methods provide the same dispersion for the bands close to the gap region (figure 3).

The dependence of the total and projected DOS on energy is shown in figure 5. It is clearly seen that the valence band is split over several parts. The narrow peaks mainly composed of the Si-s states are located at −10, −9.6, −9, −8.1, −7.4, −5.7 and −4.9 eV. The Si-p states also appear in the last three peaks (from −7.4 to −4.9 eV) leading to the sp-hybridization. The rather wide part extends from −4.4 eV to the Fermi energy and the bonding Si-p and Ca-d states play a dominant role here. The Ca-s, Ca-p and Si-d states do not provide sizeable contributions in the valence band.

Let us now discuss the origin of the localized peaks (from −10 to −4.9 eV) in the density of states. It can stem from the fact that Si atoms form specific units—the trigonal starts (see figures 2 and 3 in [4])—which can be considered as Zintl anions. The formation of such units occurs because of the superposition of the Ca and Si subcages. In fact, interatomic Ca–Ca distances in pure Ca (3.95 Å) and in Ca_3Si_4 (3.58–4.03 Å) are relatively close, allowing Si atoms to be built in as clusters in the Ca subcage. Similar features have been observed for Ca_2Si [2]. As we have mentioned above, the last valence and the first conduction bands are characterized by the loop of extrema leading locally to small band dispersion. This, in turn, gives rise to an abrupt reduction of the density of states near the Fermi level.

3.3. Transport properties

To provide a link between band structure and transport properties, the effective mass tensor for electrons and holes using the obtained band structure data was calculated. The electron masses along the principal axes were calculated at the conduction band minimum in the **k**-point situated along the K–M direction, while the hole masses were calculated at the valence band maximum in the **k**-point along the Γ–T2 direction (indicated by the arrow in figure 3). The second derivatives of the energy were calculated by using the five and higher number of points scheme. The principal axis components of the carrier effective mass tensor are represented in table 3.

The most important feature is that the specific topology of the loops of extrema always provides a large value for some of the components of the effective mass tensor, namely the m_{yy} (m_{xx}) for the holes (electrons) due to the almost flat bands along the corresponding directions (see figure 4). A similar situation for the effective mass anisotropy was previously observed for $ReSi_{1.75}$ [11] and β–$FeSi_2$ [12] where one of the bands had a very small dispersion along some direction. This in its turn should lead to a great anisotropy of the transport properties in Ca_3Si_4.

If one assumes the contributions of different scattering mechanisms to be independent, the total mobility according to the Mathiessen approximation is $\mu^{-1} = \sum_i \mu_i^{-1}$, where i stands for the different scattering mechanisms under consideration. In our case we assumed $\mu^{-1} = \mu_{\mathrm{AC}}^{-1} + \mu_{\mathrm{NPO}}^{-1} + \mu_{\mathrm{PO}}^{-1} + \mu_{\mathrm{IM}}^{-1} + \mu_{\mathrm{IMO}}^{-1}$, where μ_{AC}, μ_{NPO}, μ_{PO}, μ_{IM}, μ_{IMO} are the carrier mobilities controlled by scattering by the acoustic lattice mode, nonpolar and polar optical modes and charged and neutral impurities, respectively. The details of the calculations are

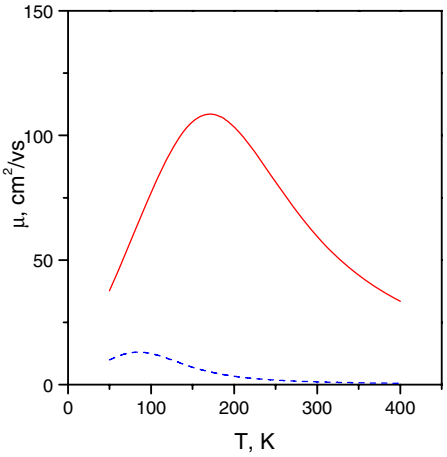

Figure 6. Mobility μ versus temperature T. The solid line corresponds to the mobility in the [0001] direction, the dashed one to the mobility in the basal plane.

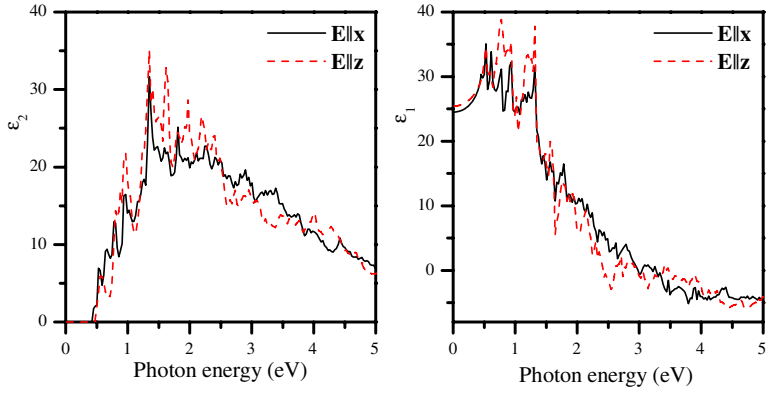

Figure 7. The imaginary (ε_2) and real (ε_1) parts of the dielectric function versus photon energy of Ca_3Si_4 for different light polarizations as calculated by FLAPW.

presented elsewhere [11, 13, 14]. The calculated hole mobility with the averaged effective mass value in the basal plane (m_{yy} was taken to be 40) and with the m_{zz} value for a reasonable set of parameters is shown in figure 6. In our calculations we used the following parameters: material density -2.47 g cm^{-3}, mean longitudinal sound velocity estimated to be 1.97×10^6 cm s^{-1}, Debye temperature of 600 K, high frequency and static dielectric constants of 5 and 25, respectively, and an ionized impurity or defect concentration of 5×10^{18} cm^{-3}.

According to our theoretical predictions the difference in the hole mobility values in the basal plane as compared with the one along the [0001] direction can reach an order of magnitude. There fore we also expect similar effects on the mobility of electrons.

3.4. Dielectric function

In figure 7 we present the dependence of the real and imaginary parts of the dielectric function of Ca_3Si_4 on photon energy. Neither the ε_2 curve nor the ε_1 curve shows any sizeable anisotropy for different light polarization, whereas for Ca_2Si the anisotropy of the optical functions is

evident [2]. For example, in the case of the imaginary part of the dielectric function of Ca_3Si_4 the curves for $\mathbf{E}\|\mathbf{x}$ and $\mathbf{E}\|\mathbf{z}$ are close in shape: a rapid start at about 0.5 eV, the main maximum at 1.1 eV followed by a slope to lower values. The rapid increase in the ε_2 curves at 0.5 eV can be attributed to the direct transitions in the L and K points in addition to another saddle point according to appreciable values of the dipole matrix elements. The static dielectric constant $\varepsilon_1(0)$ is about 25 for Ca_3Si_4, and larger than 16 for Ca_2Si [2].

4. Conclusions

In this paper we have predicted that Ca_3Si_4 is a semiconducting material with an indirect band-gap of 0.35 eV. Our calculations have been performed without the GW approximation and an underestimation of the gap value is expected. We believe that the 'real' gap can be as large as 0.6 eV and this issue should be checked experimentally. In addition, both the last valence band and the first conduction band possess a loop of extrema instead of common band dispersion with maximum/minimum in a **k**-point. Because of the loop of extrema we have revealed a large anisotropy of the effective masses for both holes and electrons. This issue in turn led to a sizeable anisotropy in the mobility of carriers. Finally, our calculations also predict the isotropic character of optical functions for this material.

References

[1] Borisenko V E 2000 *Semiconducting Silicides* (Berlin: Springer)
[2] Migas D B, Miglio L, Shaposhnikov V L and Borisenko V E 2003 *Phys. Rev.* B **67** 205203
[3] Lebegue S, Arnaud B and Alouani M 2005 *Phys. Rev.* B **72** 085103
[4] Manfrinetti P, Fornasini M L and Palenzona A 2000 *Intermetallics* **8** 223
[5] Kresse G and Hafner J 1994 *Phys. Rev.* B **49** 14251
[6] Kresse G and Furthmüller J 1996 *J. Comput. Mater. Sci.* **6** 15
Kresse G and Furthmüller J 1996 *Phys. Rev.* B **54** 11169
[7] Perdew J and Zunger A 1981 *Phys. Rev.* B **23** 5048
[8] Perdew J and Wang Y 1992 *Phys. Rev.* B **45** 13244
[9] Blaha P, Schwarz K, Madsen G K H, Kvasnicka D and Luitz J 2001 *WIEN2k, An Augmented Plane Wave + Local Orbitals Program for Calculating Crystal Properties (Karlheinz Schwarz, Techn. Universität Wien, Austria)* ISBN 3-9501031-1-2
[10] Moroni E G, Wolf W, Hafner J and Podloucky R 1999 *Phys. Rev.* B **59** 12860
[11] Ivanenko L, Shaposhnikov V L, Filonov A B, Migas D B, Behr G, Werner J, Schumann J, Vinzelberg H and Borisenko V 2002 *Microelectron. Eng.* **64** 225
[12] Martinelli L, Grilli E, Migas D B, Miglio L, Marabelli F, Soci C, Geddo M, Grimaldi M G and Spinella C 2002 *Phys. Rev.* B **66** 085320
[13] Ivanenko L, Filonov A, Shaposhnikov V, Behr G, Souptel D, Schumann J, Vinzelberg H, Plotnikov A and Borisenko V 2003 *Microelectron. Eng.* **70** 209
[14] Filonov A B, Tralle I E, Migas D B, Shaposhnikov V L and Borisenko V E 1997 *Phys. Status Solidi* b **203** 183